DOI: 10.1113/JP276935

Accepted Article

Confidential draft; not for distribution 10/3/18

The central amygdala to periaqueductal gray pathway comprises intrinsically distinct neurons differentially affected in a model of inflammatory pain.

Jun-Nan Li[1,2] and Patrick L. Sheets[1,2]

[1]Department of Pharmacology and Toxicology, [2]Stark Neurosciences Research Institute, Indiana University School of Medicine, Indianapolis, IN, 46202;

Address correspondence to: Patrick L. Sheets, Ph.D., Indiana University School of Medicine, Neuroscience Research Building 400D, 320 West 15th St, Indianapolis, IN 46202; email: plsheets@iupui.edu; phone: 317-278-6383.

Abbreviated title: Distinct CeA-PAG neurons affected by inflammatory pain

Key words: central amygdala, periaqueductal gray, inflammatory pain, electrophysiology, brain slice

Table of Contents category: Neuroscience

Author contributions: P.L.S. designed research with input from J.L.; J.L. performed all experiments. J.L. and P.L.S. analyzed data and wrote the paper.

Acknowledgements: The authors thank Brianna Mork and Andrea Jones for support with experiments and data analysis.

This is the author's manuscript of the article published in final edited form as:

Li, J.-N., & Sheets, P. L. (2018). The central amygdala to periaqueductal gray pathway comprises intrinsically distinct neurons differentially affected in a model of inflammatory pain. The Journal of Physiology, 0(ja). https://doi.org/10.1113/JP276935

Accepted Article

Conflicts of interest: The authors declare no competing financial interests.

Key points:

- The central nucleus of the amygdala (CeA) encompasses the main output pathways of the amygdala, a temporal lobe structure essential in affective and cognitive dimensions of pain.
- A major population of neurons in the CeA send projections to the periaqueductal gray (PAG), a key midbrain structure that mediates coping strategies in response to threat or stress.
- CeA-PAG neurons are topographically organized based on their targeted subregion within the PAG.
- PAG-projecting neurons in the central medial (CeM) and central lateral (CeL) regions of CeA are intrinsically distinct.
- CeL-PAG neurons are a homogeneous population of intrinsically distinct neurons while CeM-PAG neurons are intrinsically heterogeneous.
- Membrane properties of distinct CeM-PAG subtypes are altered in the Complete Freund's Adjuvant (CFA) model of inflammatory pain.

Abstract

Background: A major population of neurons in the central nucleus of amygdala (CeA) send projections to the periaqueductal gray (PAG), a key midbrain structure that mediates coping strategies in response to threat or stress. While the CeA-PAG pathway has proved to be a

This article is protected by copyright. All rights reserved.

Accepted Article

component of descending antinociceptive circuitry, the functional organization of CeA-PAG neurons remains unclear.

Study design: We identified CeA-PAG neurons in C57BL/6 mice of both sexes using intracranial injection of fluorescent retrograde tracer into the PAG. In acute brain slice, we investigated the topographical and intrinsic characteristics of retrogradely-labeled CeA-PAG neurons using epifluorescence and whole-cell electrophysiology. We also measured changes to CeA-PAG neurons in the Complete Freund's Adjuvant (CFA) model of inflammatory pain.

Results: Neurons in the central lateral (CeL) and central medial (CeM) amygdala project primarily to different regions of the PAG. CeL-PAG neurons are comprised of a relatively homogeneous population of intrinsically distinct neurons while CeM-PAG neurons are intrinsically heterogeneous. Membrane properties of distinct CeM-PAG subtypes are altered one day following induction of CFA inflammatory pain model.

Conclusion: Collectively, our results provide insight into pain-induced changes to a specific population of CeA neurons that likely play a key role in the integration of noxious input with endogenous analgesia and behavioral coping response.

Introduction

The amygdala is a temporal lobe structure essential in affective and cognitive dimensions of pain. The central nucleus of the amygdala (CeA) encompasses the main output pathways of the amygdala. The rodent CeA can be broadly divided into a lateral (CeL) and a medial (CeM) subregion (McDonald, 1982). The CeL can be further subdivided

This article is protected by copyright. All rights reserved.

Accepted Article

into a lateral-capsular division (CElc), an intermediate division (CEi) and a lateral division proper (CEl) based on anatomical and immunohistochemical organization (McDonald, 1982; Cassell *et al.*, 1986; Jolkkonen & Pitkanen, 1998). Studies demonstrate that CeA is predominantly composed of GABAergic inhibitory neurons and essential for fear conditioning. The CeM is the major output nucleus of the amygdala projecting to regions important for behavioral and physiological responses to emotionally relevant events (Hopkins & Holstege, 1978; Pape & Pare, 2010). However, more recent data show that CeL neurons also send GABAergic projections to behavioral and physiologic effector regions (Penzo *et al.*, 2014). Functionally, CeL is required for fear acquisition, whereas conditioned fear responses are driven by output neurons in the CeM. The CeL to CeM pathway is proposed to gate fear expression and regulate fear generalization (Ciocchi *et al.*, 2010). Electrophysiological recordings from rodents clearly show that there are intrinsically distinct subpopulations of CeA neurons (Schiess *et al.*, 1999; Dumont *et al.*, 2002; Haubensak *et al.*, 2010). However, a clear organizing principle for these subpopulations remains unclear. We hypothesized that long-range projection target corresponds to the intrinsic identity of CeA neurons as seen with cortical pyramidal neurons (Le Be *et al.*, 2007; Dembrow *et al.*, 2010; Sheets *et al.*, 2011; Ferreira *et al.*, 2015). Therefore, we aimed to investigate whether a major output pathway of the CeA consists of a homogeneous population of neurons.

Neurons in the CeA send projections to the periaqueductal gray (PAG) (LeDoux *et al.*, 1988; Rizvi *et al.*, 1991; da Costa Gomez & Behbehani, 1995). The PAG is a midbrain structure that integrates motivational/limbic and sensory input to initiate specific outputs including coping behavior (Bandler & Carrive, 1988; Bandler & Depaulis, 1988; De Oca *et al.*, 1998). Specifically in the caudal PAG, excitation of the dorsolateral and lateral column induces the flight, tachycardia, hypertension responses and short-term (non-opioid mediated) analgesia seen in response to a threat (Bandler & Carrive, 1988; Bandler &

This article is protected by copyright. All rights reserved.

Accepted Article

Depaulis, 1988; LeDoux *et al.*, 1988). In contrast, activating ventrolateral column drives a contrasting response involving quiescence, bradycardia, hypotension, and opioid mediated analgesia (Bandler & Shipley, 1994; Bandler *et al.*, 2000). Reciprocal signaling between the PAG and amygdala (Rizvi *et al.*, 1991) is critical for neuronal processing of nociceptive input (Behbehani, 1995), fear conditioning (McNally *et al.*, 2011; Penzo *et al.*, 2014) and defensive behavior (Tovote *et al.*, 2016). While previous research has studied the CeA-PAG pathway, little remains known about the organization and physiology of CeA neurons projecting to the PAG. Applying anatomical labeling strategies and whole cell recordings in acute brain slice, we aimed to identify and characterize retrogradely-labeled PAG-projecting CeA neurons (CeA-PAG neurons).

The CeA is termed the 'nociceptive amygdala' (Neugebauer, 2015) as extensive research shows that CeA neurons are sensitized in models of inflammatory (Neugebauer & Li, 2003; Neugebauer *et al.*, 2003; Li & Neugebauer, 2004a, b, 2006; Ji & Neugebauer, 2007; Ji *et al.*, 2009) and neuropathic pain (Ikeda *et al.*, 2007; Goncalves & Dickenson, 2012). Recent evidence suggests acute pain activates ***distinct*** populations of CeA neurons (Butler *et al.*, 2017). Therefore, we also aimed to determine changes to the excitability of CeA-PAG neurons in the complete Freund's adjuvant (CFA) model of inflammatory pain. Here we present data showing that CeA-PAG neurons are intrinsically heterogeneous and that subpopulations of CeA-PAG neurons are differentially altered in the CFA model of inflammatory pain. Overall, our data produce insight into pain-induced changes to specific CeA neurons that likely play a key and distinct role in the integration of noxious input with endogenous analgesia and behavioral coping responses.

Methods

This article is protected by copyright. All rights reserved.

Accepted Article

Ethical Approval

The Institutional Animal Use and Care Committee (IACUC) of the Indiana University School of Medicine approved all procedures and experiments presented in this study.

Animals

Wild-type C57BL/6 mice (Jackson Laboratory) of both sexes were used for this study in accordance with the animal care and use guidelines of Indiana University, the National Institutes of Health, and the Society for Neuroscience. A majority of mice used for these studies were bred in-house, but in cases where there were lapses in pups from our breeding colony, mice were purchased from Jackson Laboratory.

Intracranial injection of retrograde tracers

At postnatal days 25-68, mice (10-22 g) of either sex were anesthetized with 1.5% isoflurane in 100% O_2 with a flow rate of 0.8 L/min (SurgiVet Isotech 4, Smith). The top of the head was shaved. The head was stabilized in a stereotaxic frame (900 series, Kopf instruments). Betadine and ethanol were used to disinfect the shaved area. Body temperature was maintained at 37 °C using a feedback-controlled heating pad (FHC). Prior to incision, buprenorphine HCl (0.03 mg/kg) was injected subcutaneously for pain relief. For PAG injection, the scalp was incised, a craniotomy was made, the dura was reflected, and pipettes were advanced to reach the stereotaxic coordinates of the desired target. The pipette was advanced to the intracranial target and submicroliter volumes (100 nL) of red IX Retrobeads™ (Lumafluor, Inc., Naples, FL) were injected at a rate of 25 nl/min using a Hamilton syringe connected to an UltraMicoPump 3 driven by a Micro 4 MicroSyringe Pump Controller (World Precision Instruments). The pipette was kept in place for 6 min to limit tracer reflux out of the injection site. The incision was closed with tissue adhesive

This article is protected by copyright. All rights reserved.

Accepted Article

(Vetbond™). Following surgery, meloxicam (5 mg/kg) was injected subcutaneously for pain relief during recovery. The animals were allowed 3-7 days of recovery before experiments. Stereotaxic coordinates for caudal PAG injections were as follows (relative to bregma): 3.4 mm caudal, 0.75 mm lateral (right), 3.9 mm deep at a 0° angle off the vertical plane. For rostral PAG injections, coordinates were (relative to bregma): 1.2 mm caudal, 0.45 mm lateral (right), 4.1 mm deep at a 0° angle off the vertical plane. For ventrolateral PAG (vlPAG) injections, the head was fixed at a 38° down angle and coordinates were (relative to lambda): 4.2 mm caudal, 0.55 mm lateral (right), 3.0 mm deep at a 52° angle off the horizontal plane. For dorsolateral PAG (dl/lPAG) injections, the head was fixed at a 38° down angle and coordinates were (relative to lambda): 3.2 mm caudal, 0.55 mm lateral (right), 2.6 mm deep at a 52° angle off the horizontal plane. Targeting of retrograde tracer into specific regions of the PAG was verified for all injections using a fluorescent stereo microscope (Leica M165 FC) to image slices of the PAG. Criteria for distinguishing PAG regions was based on the atlas The Mouse Brain in Stereotaxic Coordinates, Second Edition (Paxinos & Franklin, 2001) which shows the total length of the PAG as 2.66 mm (from -2.54 mm to -5.20 mm relative to bregma). For our criteria, we defined rostral PAG as the PAG region -2.54 mm to -3.52 mm from bregma, and we defined the caudal PAG as the PAG region -4.36 mm to -5.20 mm from bregma. Injections to the dl/lPAG and the vlPAG were only included if they were contained with the defined caudal PAG region.

Acute brain slice preparation

After brief anesthetization by isoflurane, injected mice were decapitated and brains were rapidly extracted (< 1 min) and placed in ice-chilled cutting solution (in mM: 110 choline chloride, 25 NaHCO3 (sodium bicarbonate), 25 D-glucose, 11.6 sodium ascorbate, 7 MgSO4 (magnesium sulfate), 3.1 sodium pyruvate, 2.5 KCl, 1.25 NaH2PO4, and 0.5 CaCl2).

This article is protected by copyright. All rights reserved.

Accepted Article

Coronal slices (300 μm) containing the amygdala and the PAG were prepared by vibratome (VT1200S, Leica), and transferred to artificial cerebrospinal solution (ACSF, in mM: 127 NaCl, 25 $NaHCO_3$, 25 D-glucose, 2.5 KCl, 2 $MgCl_2$, 2 $CaCl_2$, and 1.25 NaH_2PO_4, aerated with 95% O_2 / 5% CO_2) at 37 °C for 30 min. Slices were subsequently incubated in ACSF at 21-22 °C for at least 45-60 minutes prior to electrophysiological recordings.

Confocal imaging of retrogradely-labeled neurons

At least 48 hours following retrograde tracer injections into specific regions of the PAG, brains were fixed by cardiac perfusion with fixative (4% paraformaldehyde in PBS). Brain sections containing amygdala and PAG were cut by vibratome at a thickness of 50 μm. Confocal fluorescent images of retrogradely-labeled CeA-PAG neurons were obtained using a Nikon Eclipse Ti inverted microscope equipped with four lasers (405 nm, 488 nm, 561 nm and 640 nm). A 10x Plan Apo λ objective was used to scan the slices from the top to bottom at 2 μm intervals. The image acquisition was conducted using NIS-Elements (Ver 5.02) software. Identification of labeled neurons in the central lateral (CeL) and central medial

(CeM) regions of the CeA was based on the atlases The Mouse Brain in Stereotaxic Coordinates, Second Edition (Paxinos & Franklin, 2001) and Allen Reference Atlas: A Digital Color Brain Atlas of the C57Black/6J Male Mouse (Dong, 2008). For each injected mouse (n = 3 mice per PAG subregion), labeled CeM-PAG and CeL-PAG were counted across 7 brain sections of the amygdala and are presented as total neurons from each group of injected animals.

This article is protected by copyright. All rights reserved.

Accepted Article

Whole-cell slice electrophysiology of retrogradely-labeled neurons

Electrophysiological recordings from fluorescently labeled CeA-PAG neurons in acute brain slice were performed in whole-cell patch-clamp configuration. Briefly, slices were transferred to the recording chamber of a SliceScopePro 6000 (Scientifica) containing an upright microscope (BX51, Olympus) and PatchStar micromanipulators (Scientifica). Brain slices were held in place with short pieces of flattened gold wire (0.813 mm diameter; Alfa Aesar). CeA-PAG neurons were identified by fluorescence of red Retrobeads™ (Lumafluor, Inc) using LED optics (coolLED). As with confocal imaging, identification of labeled neurons in the central lateral (CeL) and central medial (CeM) regions of the CeA was based on the atlases The Mouse Brain in Stereotaxic Coordinates, Second Edition (Paxinos & Franklin, 2001) and Allen Reference Atlas: A Digital Color Brain Atlas of the C57Black/6J Male Mouse (Dong, 2008). Pipettes for recordings were fabricated from borosilicate capillaries with filaments (G150-F, Warner) using a horizontal puller (P-97, Sutter), and filled with intracellular solution composed of (in mM) 128 K-gluconate, 10 HEPES (4-(2-Hydroxyethyl)piperazine-1-ethanesulfonic acid), 1 EGTA (Ethylene-bis(oxyethylenenitrilo)tetraacetic acid), 4 $MgCl_2$ (magnesium chloride), 4 ATP (adenosine 5'-triphosphate disodium salt), and 0.4 GTP (guanosine 5′-triphosphate sodium salt hydrate), 10 phosphocreatine, 3 ascorbate, and 0.05 Alexa-594 or 488 (MolecularProbes); pH 7.3. EGTA was included both to facilitate seal formation and to reduce cytosolic calcium elevations induced by the various stimulus protocols used in these studies. Artificial cerebrospinal fluid (ACSF) was used as the extracellular recording solution. Slices were ideally used 1.5–3 h after preparation, but some were used up to 6 h after preparation. Recordings were performed in 31-33 °C ACSF, which was refreshed every 2 hours. The recording temperature was controlled by an in-line heating system (TC324B, Warner). Recordings were targeted to labeled neurons 60–100 μm deep in the slice. Intrinsic

This article is protected by copyright. All rights reserved.

Accepted Article

recordings were performed with synaptic blockers (in μM): 5 CPP (-((R)-2-Carboxypiperazin-4-yl)-propyl-1-phosphonic acid), 10 NBQX (2,3-Dioxo-6-nitro-1,2,3,4-tetrahydrobenzo[*f*]quinoxaline-7-sulfonamide), and 5 GABAzine (6-Imino-3-(4-methoxyphenyl)-1(6*H*)-pyridazinebutanoic acid hydrobromide). Pipette capacitance was compensated; series resistance (Rs) was monitored but not compensated, and required to be ≤ 35 MΩ for inclusion in the data set. Current-clamp recordings were bridge-balanced. Current was injected as needed to maintain the membrane potential near -70 mV during select stimulus protocols (i.e., within the activation range of I_h at baseline). Recordings were amplified and filtered at 4 kHz and digitized at 10 kHz using a Multiclamp 700B amplifier (Molecular Devices). Membrane potential values were not corrected for a calculated liquid junction potential of 11 mV (32-33 °C). Ephus software was used for data collection (Suter *et al.*, 2010).

Voltage sag and input resistance were measured from a membrane potential of -70 ± 3 mV. Voltage sag was measured by presenting multiple one second hyperpolarizing current steps (-200 pA, -150 pA, -100 pA, -50 pA). Percentage voltage sag was calculated using the peak voltage (V_{peak}) and steady-state voltage (V_{ss}) using the equation $100 \times (V_{peak}–V_{ss})/V_{peak}$. Input resistance was measured from the steady-state responses to a series of hyperpolarizing and subthreshold depolarizing current steps (duration 1.0 s, amplitude -200 to 100 pA, 50 pA steps), as the slope of a linear least-squares fit to the resulting voltage–current relationship. Current threshold for action potentials (APs) was defined as the magnitude of current step that produced at least one AP. Voltage threshold (in mV) for APs was defined as the point when d*V*/d*t* exceeded 10% of its maximum value, relative to a d*V*/d*t* baseline measured 2 ms before the AP peak, which was measured as the maximum membrane potential reached after threshold. The AP amplitude was determined by the difference between threshold and peak values. The AP half-width was measured at half-

This article is protected by copyright. All rights reserved.

Accepted Article

amplitude. Onset of AP firing was measured as the time (in msec) between current step initiation and threshold of the first AP. Frequency–current relationships were calculated from the numbers of APs per current step, and frequency–current slopes were calculated by linear regression. Spike (or AP) frequency adaptation (SFA) was obtained by acquiring the ratio of the 3rd interspike interval (ISI) over the 5th ISI (fast-SFA) and the ratio of the 5th ISI over the 10th ISI (slow-SFA). Fast and slow SFA were calculated from responses that produce more than five and ten APs, respectively.

Inflammatory pain model

Complete Freund's Adjuvant (CFA), obtained from Sigma Aldrich (F5881), is a heat-killed bacterial suspension that creates an immune response at the site of the injection. When CFA is injected intracutaneously (27G needle or smaller) into the plantar surface of the hindpaw, it produces a robust model of inflammatory pain (Corder *et al.*, 2013). For these experiments, we intracutaneously injected CFA (10 µL, 1 mg/mL) into the plantar surface of the left hindpaw.

Assessment of inflammatory pain behavior

Mice (postnatal day 27-51) were acclimated to the pain testing behavior apparatus, behavioral suite, and experimenter before the von Frey filament paw-withdrawal threshold is established. Acclimation entailed placing the mouse inside clear 6-inch vertical plastic tube (4-inch internal diameter) on top of a wire mesh platform (exposing the hindpaws for testing). Mice were acclimated for two non-consecutive days for a half hour each day prior to recording baseline withdrawal thresholds. Baseline withdrawal threshold (for both hindpaws) was established prior to CFA or saline injection by following the 'simplified up-down' or SUDO method (Bonin *et al.*, 2014). On post-injection day one (PID-1), the SUDO method

This article is protected by copyright. All rights reserved.

Accepted Article

was used to assess mechanical allodynia, both ipsilateral and contralateral to the injury. Experimenters were blinded to treatment groups (saline vs. CFA) during behavioral testing. Using standard von Frey filaments 2-9 (filament 1: 0.008g; filament 2: 0.02 g; filament 3: 0.07 g; filament 4: 0.16 g; filament 5: 0.4 g; filament 6: 1 g; filament 7: 2 g; filament 8: 6 g) testing began with the middle filament (filament 4). The pressure from the filament was applied to midplantar surface of the hind paw for 3 seconds and behavior responses such as hind paw retraction, paw licking, or shaking was considered as nocifensive behavior, and classified as a pain-response (Martinov *et al.*, 2013). If the applied filament did not elicit a response the next higher filament was used, if a response is elicited, the next lower filament was used until the 5th and final filament was presented. This method minimized the number of filament presentations to the mouse and maximize score sensitivity. On day of slice experiments, a final withdrawal testing was performed, with the mouse being euthanized immediately after.

Statistical analysis

Custom MATLAB (Mathworks, Natick, MA) routines were used to analyze data off-line. For all data, a Lilliefors test was performed prior to significance testing to determine if the data were normally distributed. Significant differences between multiple independent groups will be determined using a one-way ANOVA for normally distributed data or a Kruskal-Wallis test for non-normally distributed data. A Bonferroni post-hoc analysis was used for multiple comparisons if the one-way ANOVA or Kruskal-Willis test resulted in a significant omnibus F test. Pairwise comparisons were performed with the Student's paired t test. Statistical comparisons between two independent groups was determined with the Student's unpaired t test (for normally distributed data) or the Wilcoxin rank sum test (for non-normally distributed data).

This article is protected by copyright. All rights reserved.

Accepted Article

Results

CeA-PAG neurons are topographically organized based on projection target within the PAG.

Activation along the rostral-caudal axis of the PAG evokes distinct coping behaviors associated with stressful stimuli (Bandler & Shipley, 1994; Bandler *et al.*, 2000; Keay & Bandler, 2001). Therefore, we targeted our tracer injections to either rostral or caudal regions of the PAG to examine retrogradely-labeled PAG-projection neurons in the amygdala (Fig. 1 *A, B*). Tracer injection into the rostral PAG (rPAG) resulted in retrograde labeling of soma primarily in the central medial amygdala (CeM; Fig. 1*C-E*). Injection of tracer spanning the entire caudal PAG consistently produced retrograde labeling of soma in both the CeM and CeL (Fig. 1*F-H*). Because our initial caudal PAG injections spanned both dorsal and ventral regions, we next targeted our tracer injections to either dorsolateral/lateral or the ventrolateral regions of the caudal PAG. Following injection of tracer into the dorsolateral/lateral PAG (dl/lPAG) the majority of labeled soma were detected primarily in the CeM with the minority found in the CeL (Fig. 1 *I-K*). In comparison, in mice with tracer injected into the ventrolateral PAG (vlPAG), labeled neurons were detected in both the CeL and CeM with the smaller portion observed in the CeM (Fig. 1 *L-N*). Overall, these results suggest that CeA-PAG neurons are topographically organized based on their targeted subregion within the PAG.

PAG-projecting neurons in CeM and CeL are intrinsically distinct.

We next targeted retrogradely-labeled CeA-PAG neurons for whole-cell electrophysiological recording in acute brain slice from naïve mice. Our analysis revealed that PAG-projecting neurons in CeM (CeM-PAG neurons) and CeL (CeL-PAG neurons) are

This article is protected by copyright. All rights reserved.

Accepted Article

intrinsically distinct. For subthreshold characteristics, CeM-PAG neurons are significantly depolarized with larger voltage sag and input resistance compared to CeL-PAG neurons (Table 1). Examination of suprathreshold properties showed that compared to CeL-PAG neurons, CeM-PAG neurons 1) have a lower current and voltage threshold for action potential (AP) firing, 2) have a shorter onset to AP firing at threshold, 3) have a shorter AP height, and 4) display spike-frequency adaptation (Table 1). One of few similarities between CeM-PAG and CeL-PAG neurons was slope of relationship between action potential (AP) frequency and current injection at threshold and twice threshold.

CeL-PAG neurons primarily display a 'late-firing' phenotype

We find that CeL-PAG neurons from naïve mice are mainly homogeneous based on their intrinsic properties (Fig. 2, Table 2). A major population of CeL-PAG neurons (n = 27/30) exhibit a delayed AP onset at firing threshold (late-firing) while a small population (n = 3/30) display a regular spiking pattern at firing threshold (Fig. 2*A, B*). Both late-firing and regular spiking neurons displayed a run-down in AP frequency at more depolarizing current steps (Fig. 2*C*). Late-firing CeL-PAG neurons have a larger fast afterhyperpolarization (fAHP) compared to regular-spiking neurons (Fig. 2*D, I*, Table 2). These data show that the majority of PAG-projecting neurons on the CeL are intrinsically similar. Surprisingly, analysis of CeL-PAG neurons based on sex revealed significant intrinsic differences (Table 4). When compared to male mice CeL-PAG neurons from female mice were hyperpolarized, expressed more voltage sag, and fired APs at a more hyperpolarized voltage threshold (Table 4). Additionally, female CeL-PAG neurons displayed narrower AP half-widths, larger AP height, and expressed less fAHP (Table 4). This analyses show that while the intrinsic phenotype (i.e. 'late-firing') is robust for CeL-PAG neurons, there is heterogeneity in the intrinsic profile of CeL-PAG 'late-firing' neurons between males and females.

This article is protected by copyright. All rights reserved.

Accepted Article

CeM-PAG neurons are intrinsically heterogeneous

Recordings from CeM-PAG neurons (Fig. 3*A, B*) from naïve mice revealed four distinct subclasses of neurons (Fig. 3*C*). Late-firing neurons comprised the smallest percentage (3/32) of CeM-PAG neurons (Fig. 3*C*). Late-firing CeM-PAG neurons display similar subthreshold and firing properties as CeL-PAG late-firing neurons (Fig. 2). The proportion of the remaining three classes was relatively equal (Fig. 3*C*). The predominant subtype (12/32) of CeM-PAG neurons display a fast-firing phenotype that does not adapt with increasing step current (Fig. 3*Diii*, Fig. 4*A*). A single AP evoked from fast-spiking CeM-PAG neurons revealed a fAHP followed by a slight depolarization and slow afterhyperpolarization (Fig. 3*Dii*). The next most populous group (10/32) exhibit a bursting AP pattern that accommodates at firing threshold and adapts with increasing step current (Fig. 3*Eiii*, Fig. 4*A*). Single APs from bursting CeM-PAG neurons display a prominent afterdepolarization followed by a slow afterhyperpolarization (Fig. 3*Eii*). The third most populous group (8/32) of CeM-PAG neurons display the regular-spiking phenotype (Fig. 3*Fiii*) that we observed in a small subset of CeL-PAG neurons (Fig. 2*B*). No afterdepolarization is observed in single APs of regular-firing CeM-PAG neurons (Fig. 3*Fii*).

All three of the predominant CeM-PAG subtypes have similar resting membrane potentials and input resistance (Fig. 4*B, C*, Table 3) while expressing measurable voltage sag when injected with a hyperpolarizing step current (Fig. 3*Di-Fi*, Fig. 4*D*, Table 3) indicating the activation of hyperpolarization-activated current (I_h). Both current and voltage threshold for AP firing were not statistically different between CeM-PAG subtypes (Fig. 4*E, F*, Table 3). Trains of APs in bursting CeM-PAG neurons adapt significantly more than trains of APs in fast-spiking CeM-PAG neurons (Fig. 4*G*, Table 3). A unique feature of fast-spiking CeM-PAG neurons was a significantly shorter AP half-width (Fig. 4*H*, Table 3). Lack of fAHP

This article is protected by copyright. All rights reserved.

Accepted Article

was defining characteristic of regular-spiking neurons (Fig. 4*I*, Table 3). Collectively, these data show that CeM-PAG neurons are a heterogeneous population thereby refuting our hypothesis that projection target correlates with intrinsic characteristics in the CeM. In contrast to CeL-PAG neurons, we find that only AP half-width of fast-spiking CeM-PAG neurons differs between sexes (Table 4).

We next examined whether intrinsic phenotype of the PAG-projecting neurons in the CeA relates to targeting of subregion within the PAG. We consistently recorded from late-firing CeL-PAG neurons following injection of tracer throughout the caudal PAG or isolated to the caudal vlPAG (Table 5). The sparse regular-spiking CeL-PAG neurons and late-firing CeM-PAG neurons were recorded following tracer injection throughout the caudal PAG (Table 5). We find the majority of fast-spiking CeM-PAG neurons following tracer injection into the caudal regions (throughout, dl/l, and vl) of the PAG, and we find the majority of regular-spiking CeM-PAG neurons following tracer injection into the rostral PAG (Table 5). The pattern of bursting CeM-PAG neurons is less defined as 50% are found following tracer injection into rostral PAG and 50% are found following tracer injection into caudal PAG (throughout and dl/l; Table 5). These data suggest that the organization of intrinsically distinct CeA-PAG neurons is related to targeting of defined regions in the PAG. Nonetheless, in-depth anatomical studies are needed to fully dissect this possibility.

The Complete Freund's Adjuvant (CFA) model of inflammatory pain differentially alters intrinsically defined CeA-PAG neurons.

We next measured changes to the intrinsic excitability of CeA-PAG subtypes in a model for inflammatory pain. First, using the same intracranial injection paradigms as described above, we injected retrograde tracer in the PAG (Fig. 5*A*). Following adequate recovery time (7 days), we intracutaneously injected CFA (10 µL, 1 mg/mL) into the plantar surface of the

This article is protected by copyright. All rights reserved.

Accepted Article

left hindpaw, which creates an immune response at the site of the injection (Fig. 5*B*). This model is advantageous because it produces a consistent mechanical allodynia one day following injection. Control conditions consisted of saline injection (10 µL) into the left hindpaw (in littermates when possible) (Fig. 5*B*). Mice injected with CFA display mechanical hypersensitivity one day after injection (Fig. 5*C*).

We first recorded retrogradely-labeled CeA-PAG neurons in the right CeL of acute brains slices from mice displaying significant mechanical allodynia one day after CFA injection (Fig. 5*D*). Retrogradely-labeled CeL-PAG neurons from saline-injected mice were recorded at the same time point (1 day) following CFA injection into the hindpaw. As seen in naïve mice, CeL-PAG neurons were found primarily following tracer injection into caudal vlPAG (Table 8) and displayed a late-firing phenotype in both saline and CFA-injected mice (Fig. 5*E*). Recordings from CeL-PAG neurons (n = 10 saline, 11 CFA) revealed no significant differences in subthreshold or suprathreshold characteristics (Fig. 5*F-K,* Table*6*). While time to AP onset at threshold was shorter in CeL-PAG neurons from CFA-injected mice, it was not statistically different (p = 0.057, *t*-test) from saline-injected mice (Fig. 5*K,* Table 6).

Next, in separate cohort of saline and CFA-injected mice (Fig. 6*A*), we recorded retrogradely-labeled CeM-PAG neurons 1 day after injection (Fig. 6*B*). As in naïve animals, we detected fast-spiking, regular-firing, and bursting CeM-PAG neurons in saline and CFA-injected animals (Fig. 6*C-E*, Table 8). Recordings show that AP firing in response to depolarizing step currents increases in fast-spiking CeM-PAG neurons in slices from CFA-injected mice, however, this is only observed when neurons are held at a membrane potential of -70 mV prior to current injection (Fig. 6*F*). No difference in AP firing initiated from resting membrane potential (Fig. 6*F, left*) is likely due to CFA-injection significantly

This article is protected by copyright. All rights reserved.

Accepted Article

hyperpolarizing resting membrane potential and increasing input resistance of fast-spiking CeM-PAG neurons (Fig. 6*G, H,* Table 7). Voltage sag, current threshold and voltage threshold measured in fast-spiking CeM-PAG neurons were similar between saline and CFA-injected animals (Fig. 6*I-K,* Table 7).

Recordings from regular-firing CeM-PAG neurons show that CFA injection significantly reduces AP firing at threshold (Fig. 6*L*) while having no effect on membrane potential, input resistance, voltage sag or current threshold (Fig. 6*M-P,* Table 7). However, CFA injection hyperpolarized voltage threshold for AP firing and delayed onset for AP firing at threshold in regular-firing CeM-PAG neurons (Fig. 6*Q,* Table 7), which was not observed in fast-spiking CeM-PAG neurons (Fig. 6*K*). Interestingly, injection of CFA did not significantly affect the intrinsic properties of bursting CeM-PAG neurons (Fig. 6*R-W,* Table 7). Collectively, these data indicate that specific subtypes of PAG-projecting neurons in the CeA are differentially altered 1 day following induction of peripheral inflammation that evokes significant mechanical allodynia.

Discussion

Evidence confirms that the central amygdala (CeA) of the rodent consists of a heterogeneous population of intrinsically distinct neurons (Schiess *et al.*, 1999; Dumont *et al.*, 2002; Duvarci & Pare, 2014). However, the functional organization of these neuronal subtypes in the CeA remains not well understood. Here, we investigated whether CeA neurons with the same projection target express similar intrinsic properties thereby providing insight into their functional roles. To identify a subpopulation of CeA neurons with a defined projection target, we injected fluorescent retrograde tracers into different subregions of the periaqueductal gray (PAG), which is a midbrain structure that integrates motivational/limbic

This article is protected by copyright. All rights reserved.

Accepted Article

and sensory input to initiate specific outputs including coping behavior (Bandler & Carrive, 1988; Bandler & Depaulis, 1988; De Oca *et al.*, 1998).

Consistent with previous studies (Rizvi *et al.*, 1991; Finnegan *et al.*, 2005; Haubensak *et al.*, 2010; Penzo *et al.*, 2014), our retrograde labeling experiments reveal that PAG-projecting neurons are distributed in the both central lateral (CeL) and central medial (CeM) subregions of the amygdala. Moreover, we show that location of our retrograde tracer with specific subregions of the PAG relates to the topographical distribution of labeled soma in the CeA. We detect labeled PAG-projecting neurons primarily in the CeL (CeL-PAG neurons) when retrograde tracer was injected into the ventrolateral region of the caudal PAG. However, we find labeled PAG-projecting neurons in the CeM (CeM-PAG neurons) following injections throughout multiple sub-regions of the PAG including rostral PAG and dorsolateral, lateral, and ventrolateral caudal PAG. This finding is interesting in that distinct regions of the PAG are devoted to the regulation of defined physiological outcomes. More specifically, the dorsolateral and lateral areas of the PAG are involved in panic, non-opioid mediated analgesia, hypertension, and tachycardia while ventrolateral areas are associated with quiescence, opioid mediated analgesia, hypotension, and bradycardia (Fardin *et al.*, 1984). Therefore, CeL-PAG and CeM-PAG neurons are topographically poised to regulate disparate behaviors elicited via activation of the PAG.

Extensive work in both rat and mouse shows that CeL neurons are intrinsically heterogeneous (Dumont *et al.*, 2002; Lopez de Armentia & Sah, 2004; Chieng *et al.*, 2006; Haubensak *et al.*, 2010; Amano *et al.*, 2012; Hou *et al.*, 2016; Hunt *et al.*, 2017). Yet, the functional organization of this heterogeneity is still emerging. Here we show we can isolate neurons displaying the distinct ‘late firing’ phenotype by recording retrogradely-labeled PAG-projecting neurons in CeL. Protein kinase C-δ (PKCδ) is expressed in a majority of ‘late-

This article is protected by copyright. All rights reserved.

Accepted Article

firing' neurons in CeL (Haubensak *et al.*, 2010) suggesting that CeL-PAG neurons in mice are PKC-δ expressing neurons. However, another study shows a majority of CeL-PAG neurons express somatostatin (SOM) with negligible expression of PKCδ (Penzo *et al.*, 2014). This is consistent with recent evidence showing minimal overlap of PKCδ mRNA and SOM mRNA expression in CeL neurons (McCullough *et al.*, 2018). Together, this suggests that late-firing CeL neurons targeting vlPAG are SOM-positive and PKCδ-negative. To note, 42% of PKC-δ-negative neurons recorded in the CeL by Haubensak *et al.,* 2010 display a late-firing phenotype. Further experiments are necessary to dissect the molecular profile of CeL neurons that send projections to vlPAG.

In contrast to CeL-PAG neurons, we find CeM-PAG neurons are intrinsically diverse. This diversity of CeM-PAG neurons may be due to widely distributed innervation targets along the rostral-caudal axis of the PAG. Activation of rostral and caudal dl/lPAG evokes confrontational and escape behaviors, respectively (Bandler & Shipley, 1994; Bandler *et al.*, 2000). We find that a majority of labeled CeM neurons following injection of tracer into caudal dl/lPAG (11/13, Table 5) display either a fast-spiking (FS) or bursting phenotype. This suggests a functional role for FS and bursting CeM-PAG neurons in modulation of escape behavior. We identify regular-spiking (RS) CeM-PAG neurons mainly after tracer injection into the rostral PAG (Table 5). This indicates that RS CeM-PAG neurons play a role in defensive-confrontational reactions to threat. While these results argue functional differences for CeM-PAG subtypes, topographical differences are not absolute. We do find FS and bursting CeM neurons that send projections to rostral PAG and a small subset of the RS CeM neurons that project to caudal PAG (Table 5). These findings illustrate the complexity of the CeM-PAG circuit and further studies using transgenic strategies are needed to dissect the function of defined CeM-PAG pathways.

This article is protected by copyright. All rights reserved.

Accepted Article

Ascending nociceptive input signals the CeA via the parabrachial nucleus (Bernard *et al.*, 1993; Gauriau & Bernard, 2002; Neugebauer *et al.*, 2003; Neugebauer *et al.*, 2004). Extensive research shows that CeA neurons are sensitized in models of inflammatory pain (Neugebauer & Li, 2003; Neugebauer *et al.*, 2003; Li & Neugebauer, 2004a, b, 2006; Carrasquillo & Gereau, 2007; Ji & Neugebauer, 2007; Ji *et al.*, 2009). Our data expand on these findings by showing altered membrane properties of distinct subtypes of CeA-PAG neurons one day following injection of CFA into the hindpaw. Specifically, CFA injection significantly hyperpolarizes FS CeM-PAG neurons while also increasing their input resistance. While hyperpolarization suggests a decrease in excitability, the increase in input resistance enhances AP firing in response to step current when membrane potential was normalized to -70 mV. Because we did not observe a significant decrease in voltage sag in FS CeM-PAG neurons, we conclude that the increase in input resistance is not a result of reduced hyperpolarization-activated current (I_h) but possibly a downregulation of a non-voltage dependent ion channel. Additionally, increased input resistance infers that response of FS CeM-PAG neurons to synaptic input is enhanced. This suggests that CFA injection to the hindpaw is sensitizing a specific class of CeA neurons that project to both the rostral and caudal dl/lPAG, which may indicate a specific supraspinal pathway for which noxious stimuli stimulates both defense and escape behavior.

Interestingly, we find that CFA injection increases the threshold of AP firing and delays onset of AP firing at threshold in RS CeM-PAG neurons while having no effect on bursting CeM-PAG neurons. These data show that intrinsic subtypes of CeM-PAG neurons are not equally altered by CFA injection into the hindpaw. A CFA induced increased in AP firing threshold indicates decreased excitability for RS CeM-PAG neurons thereby attenuating output to PAG regions responsible for defensive-confrontational reactions to external threat. Together, this shows that CFA injection may be evoking CeA pathways that modulate

This article is protected by copyright. All rights reserved.

Accepted Article

escape behavior while suppressing those involved in defense responses. Of course, more studies are needed to understand the functional role of RS and FS CeM-PAG pathways including whether inputs serve to inhibit or disinhibit output from specific PAG subregions. Additionally, optogenetic strategies aimed at elucidating the targeting of parabrachial nucleus to specific CeA-PAG subpopulations will be essential for understanding how CFA injection is altering ascending nociceptive input to defined CeA neurons.

One limitation to this study is that we cannot determine if the intrinsic identity of CeA-PAG neurons changes following CFA injection (i.e. bursting to fast-spiking). Given we have a heterogeneous population of neurons in CeM, it is difficult to state with certainty if a neuron recorded in the CFA group was intrinsically different prior to CFA injection. In future studies, our goal is to use transgenic strategies to identify CeA-PAG neurons by molecular marker (i.e. SOM+, PKC-δ+) and by retrograde tracer. While our recordings are at relatively early time point following CFA injection, evidence shows that activation of extracellular signal-related kinase (ERK) can be detected in CeA neurons hours following induction of persistent inflammatory pain by formalin injection into the hindpaw (Carrasquillo & Gereau, 2007). However, increased ERK signaling was detected in the capsular subdivision of the CeA, which we identify as part of the CeL in this study. We do not identify significant intrinsic changes to CeL-PAG neurons following CFA injection for which there are the following possible explanations. The first is that ERK-activated neurons following formalin injection do not include CeL-PAG neurons. The second is that ERK activation is transient, and we are recording at a time point at which ERK effects have subsided. Third is that ERK activation does not significantly change intrinsic excitability. The last possibility is that the formalin and CFA models of inflammatory pain evoke mechanistically distinct changes to CeA neurons. Nonetheless, our future studies will involve identifying ERK activation in CeA-PAG neurons.

This article is protected by copyright. All rights reserved.

Accepted Article

Overall, our results demonstrate that the CeA-PAG pathway consists of a heterogeneous population of topographically and intrinsically distinct neurons, which are differentially altered in the CFA model of inflammatory pain. These findings produce new insight into pain-induced changes to specific subclasses of CeA neurons that likely play a key and distinct role in the integration of noxious input with relevant coping behaviors and descending pain inhibition.

References

Amano T, Amir A, Goswami S & Pare D. (2012). Morphology, PKCdelta expression, and synaptic responsiveness of different types of rat central lateral amygdala neurons. *J Neurophysiol* **108,** 3196-3205.

Bandler R & Carrive P. (1988). Integrated defence reaction elicited by excitatory amino acid microinjection in the midbrain periaqueductal grey region of the unrestrained cat. *Brain Res* **439,** 95-106.

Bandler R & Depaulis A. (1988). Elicitation of intraspecific defence reactions in the rat from midbrain periaqueductal grey by microinjection of kainic acid, without neurotoxic effects. *Neurosci Lett* **88,** 291-296.

Bandler R, Keay KA, Floyd N & Price J. (2000). Central circuits mediating patterned autonomic activity during active vs. passive emotional coping. *Brain Res Bull* **53,** 95-104.

Bandler R & Shipley MT. (1994). Columnar organization in the midbrain periaqueductal gray: modules for emotional expression? *Trends Neurosci* **17,** 379-389.

Behbehani MM. (1995). Functional characteristics of the midbrain periaqueductal gray. *Prog Neurobiol* **46,** 575-605.

This article is protected by copyright. All rights reserved.

Accepted Article

Bernard JF, Alden M & Besson JM. (1993). The organization of the efferent projections from the pontine parabrachial area to the amygdaloid complex: a Phaseolus vulgaris leucoagglutinin (PHA-L) study in the rat. *J Comp Neurol* **329,** 201-229.

Bonin RP, Bories C & De Koninck Y. (2014). A simplified up-down method (SUDO) for measuring mechanical nociception in rodents using von Frey filaments. *Molecular pain* **10,** 26.

Butler RK, Ehling S, Barbar M, Thomas J, Hughes MA, Smith CE, Pogorelov VM, Aryal DK, Wetsel WC & Lascelles BDX. (2017). Distinct neuronal populations in the basolateral and central amygdala are activated with acute pain, conditioned fear, and fear-conditioned analgesia. *Neurosci Lett* **661,** 11-17.

Carrasquillo Y & Gereau RWt. (2007). Activation of the extracellular signal-regulated kinase in the amygdala modulates pain perception. *J Neurosci* **27,** 1543-1551.

Cassell MD, Gray TS & Kiss JZ. (1986). Neuronal architecture in the rat central nucleus of the amygdala: a cytological, hodological, and immunocytochemical study. *J Comp Neurol* **246,** 478-499.

Chieng BC, Christie MJ & Osborne PB. (2006). Characterization of neurons in the rat central nucleus of the amygdala: cellular physiology, morphology, and opioid sensitivity. *J Comp Neurol* **497,** 910-927.

Ciocchi S, Herry C, Grenier F, Wolff SB, Letzkus JJ, Vlachos I, Ehrlich I, Sprengel R, Deisseroth K, Stadler MB, Muller C & Luthi A. (2010). Encoding of conditioned fear in central amygdala inhibitory circuits. *Nature* **468,** 277-282.

Corder G, Doolen S, Donahue RR, Winter MK, Jutras BL, He Y, Hu X, Wieskopf JS, Mogil JS, Storm DR, Wang ZJ, McCarson KE & Taylor BK. (2013). Constitutive mu-opioid receptor activity leads to long-term endogenous analgesia and dependence. *Science* **341,** 1394-1399.

This article is protected by copyright. All rights reserved.

Accepted Article

da Costa Gomez TM & Behbehani MM. (1995). An electrophysiological characterization of the projection from the central nucleus of the amygdala to the periaqueductal gray of the rat: the role of opioid receptors. *Brain Res* **689,** 21-31.

De Oca BM, DeCola JP, Maren S & Fanselow MS. (1998). Distinct regions of the periaqueductal gray are involved in the acquisition and expression of defensive responses. *J Neurosci* **18,** 3426-3432.

Dembrow NC, Chitwood RA & Johnston D. (2010). Projection-specific neuromodulation of medial prefrontal cortex neurons. *J Neurosci* **30,** 16922-16937.

Dong HW. (2008). *Allen Reference Atlas: A Digital Color Brain Atlas of the C57Black/6J Male Mouse*. John Wiley & Sons, Inc., Hoboken, NJ.

Dumont EC, Martina M, Samson RD, Drolet G & Pare D. (2002). Physiological properties of central amygdala neurons: species differences. *The European journal of neuroscience* **15,** 545-552.

Duvarci S & Pare D. (2014). Amygdala microcircuits controlling learned fear. *Neuron* **82,** 966-980.

Fardin V, Oliveras JL & Besson JM. (1984). A reinvestigation of the analgesic effects induced by stimulation of the periaqueductal gray matter in the rat. I. The production of behavioral side effects together with analgesia. *Brain Res* **306,** 105-123.

Ferreira AN, Yousuf H, Dalton S & Sheets PL. (2015). Highly differentiated cellular and circuit properties of infralimbic pyramidal neurons projecting to the periaqueductal gray and amygdala. *Frontiers in cellular neuroscience* **9,** 161.

This article is protected by copyright. All rights reserved.

Accepted Article

Finnegan TF, Chen SR & Pan HL. (2005). Effect of the {mu} opioid on excitatory and inhibitory synaptic inputs to periaqueductal gray-projecting neurons in the amygdala. *The Journal of pharmacology and experimental therapeutics* **312,** 441-448.

Gauriau C & Bernard JF. (2002). Pain pathways and parabrachial circuits in the rat. *Experimental physiology* **87,** 251-258.

Goncalves L & Dickenson AH. (2012). Asymmetric time-dependent activation of right central amygdala neurones in rats with peripheral neuropathy and pregabalin modulation. *The European journal of neuroscience* **36,** 3204-3213.

Haubensak W, Kunwar PS, Cai H, Ciocchi S, Wall NR, Ponnusamy R, Biag J, Dong HW, Deisseroth K, Callaway EM, Fanselow MS, Luthi A & Anderson DJ. (2010). Genetic dissection of an amygdala microcircuit that gates conditioned fear. *Nature* **468,** 270-276.

Hopkins DA & Holstege G. (1978). Amygdaloid projections to the mesencephalon, pons and medulla oblongata in the cat. *Experimental brain research Experimentelle Hirnforschung Experimentation cerebrale* **32,** 529-547.

Hou WH, Kuo N, Fang GW, Huang HS, Wu KP, Zimmer A, Cheng JK & Lien CC. (2016). Wiring Specificity and Synaptic Diversity in the Mouse Lateral Central Amygdala. *J Neurosci* **36,** 4549-4563.

Hunt S, Sun Y, Kucukdereli H, Klein R & Sah P. (2017). Intrinsic Circuits in the Lateral Central Amygdala. *eNeuro* **4**.

Ikeda R, Takahashi Y, Inoue K & Kato F. (2007). NMDA receptor-independent synaptic plasticity in the central amygdala in the rat model of neuropathic pain. *Pain* **127,** 161-172.

This article is protected by copyright. All rights reserved.

Accepted Article

Ji G, Horvath C & Neugebauer V. (2009). NR2B receptor blockade inhibits pain-related sensitization of amygdala neurons. *Molecular pain* **5,** 21.

Ji G & Neugebauer V. (2007). Differential effects of CRF1 and CRF2 receptor antagonists on pain-related sensitization of neurons in the central nucleus of the amygdala. *J Neurophysiol* **97,** 3893-3904.

Jolkkonen E & Pitkanen A. (1998). Intrinsic connections of the rat amygdaloid complex: projections originating in the central nucleus. *J Comp Neurol* **395,** 53-72.

Keay KA & Bandler R. (2001). Parallel circuits mediating distinct emotional coping reactions to different types of stress. *Neurosci Biobehav Rev* **25,** 669-678.

Le Be JV, Silberberg G, Wang Y & Markram H. (2007). Morphological, electrophysiological, and synaptic properties of corticocallosal pyramidal cells in the neonatal rat neocortex. *Cereb Cortex* **17,** 2204-2213.

LeDoux JE, Iwata J, Cicchetti P & Reis DJ. (1988). Different projections of the central amygdaloid nucleus mediate autonomic and behavioral correlates of conditioned fear. *J Neurosci* **8,** 2517-2529.

Li W & Neugebauer V. (2004a). Block of NMDA and non-NMDA receptor activation results in reduced background and evoked activity of central amygdala neurons in a model of arthritic pain. *Pain* **110,** 112-122.

Li W & Neugebauer V. (2004b). Differential roles of mGluR1 and mGluR5 in brief and prolonged nociceptive processing in central amygdala neurons. *J Neurophysiol* **91,** 13-24.

Li W & Neugebauer V. (2006). Differential changes of group II and group III mGluR function in central amygdala neurons in a model of arthritic pain. *J Neurophysiol* **96,** 1803-1815.

This article is protected by copyright. All rights reserved.

Accepted Article

Lopez de Armentia M & Sah P. (2004). Firing properties and connectivity of neurons in the rat lateral central nucleus of the amygdala. *J Neurophysiol* **92,** 1285-1294.

Martinov T, Mack M, Sykes A & Chatterjea D. (2013). Measuring changes in tactile sensitivity in the hind paw of mice using an electronic von Frey apparatus. *Journal of visualized experiments : JoVE***,** e51212.

McCullough KM, Morrison FG, Hartmann J, Carlezon WA, Jr. & Ressler KJ. (2018). Quantified Coexpression Analysis of Central Amygdala Subpopulations. *eNeuro* **5**.

McDonald AJ. (1982). Cytoarchitecture of the central amygdaloid nucleus of the rat. *J Comp Neurol* **208,** 401-418.

McNally GP, Johansen JP & Blair HT. (2011). Placing prediction into the fear circuit. *Trends Neurosci* **34,** 283-292.

Neugebauer V. (2015). Amygdala pain mechanisms. *Handbook of experimental pharmacology* **227,** 261-284.

Neugebauer V & Li W. (2003). Differential sensitization of amygdala neurons to afferent inputs in a model of arthritic pain. *J Neurophysiol* **89,** 716-727.

Neugebauer V, Li W, Bird GC, Bhave G & Gereau RWt. (2003). Synaptic plasticity in the amygdala in a model of arthritic pain: differential roles of metabotropic glutamate receptors 1 and 5. *J Neurosci* **23,** 52-63.

Neugebauer V, Li W, Bird GC & Han JS. (2004). The amygdala and persistent pain. *The Neuroscientist : a review journal bringing neurobiology, neurology and psychiatry* **10,** 221-234.

This article is protected by copyright. All rights reserved.

Accepted Article

Pape HC & Pare D. (2010). Plastic synaptic networks of the amygdala for the acquisition, expression, and extinction of conditioned fear. *Physiol Rev* **90,** 419-463.

Paxinos G & Franklin KBJ. (2001). *The mouse brain in stereotaxic coordinates*. Academic Press, London.

Penzo MA, Robert V & Li B. (2014). Fear Conditioning Potentiates Synaptic Transmission onto Long-Range Projection Neurons in the Lateral Subdivision of Central Amygdala. *J Neurosci* **34,** 2432-2437.

Rizvi TA, Ennis M, Behbehani MM & Shipley MT. (1991). Connections between the central nucleus of the amygdala and the midbrain periaqueductal gray: topography and reciprocity. *J Comp Neurol* **303,** 121-131.

Schiess MC, Callahan PM & Zheng H. (1999). Characterization of the electrophysiological and morphological properties of rat central amygdala neurons in vitro. *Journal of neuroscience research* **58,** 663-673.

Sheets PL, Suter BA, Kiritani T, Chan CS, Surmeier DJ & Shepherd GM. (2011). Corticospinal-specific HCN expression in mouse motor cortex: Ih-dependent synaptic integration as a candidate microcircuit mechanism involved in motor control. *J Neurophysiol*.

Suter BA, O'Connor T, Iyer V, Petreanu LT, Hooks BM, Kiritani T, Svoboda K & Shepherd GM. (2010). Ephus: multipurpose data acquisition software for neuroscience experiments. *Front Neural Circuits* **4,** 100.

Tovote P, Esposito MS, Botta P, Chaudun F, Fadok JP, Markovic M, Wolff SB, Ramakrishnan C, Fenno L, Deisseroth K, Herry C, Arber S & Luthi A. (2016). Midbrain circuits for defensive behaviour. *Nature* **534,** 206-212.

This article is protected by copyright. All rights reserved.

Accepted Article

Figure legends

Figure 1. Topographical distribution of CeA-PAG neurons. A: Schematic depicting injection of fluorescent beads into the periaqueductal gray (PAG). **B:** Diagram of coronal slice showing location of right amygdala. **C:** Retrograde tracer into the rostral PAG (D: dorsal; M: medial) resulted in (**D**) fluorescent retrograde labeling of neurons primarily in the central medial amygdala (CeM). **E:** Percentage and number of labeled neurons identified (n = 888 total) in the CeM and central lateral amygdala (CeL) following retrograde tracer injection into rostral PAG. **F:** Retrograde tracer injected throughout the PAG resulted in (**G**) fluorescent retrograde labeling of neurons in both CeM and CeL. **H:** Percentage and number of labeled neurons identified (n = 1362 total) in the CeM and CeL following retrograde tracer injection throughout the caudal PAG. **I:** Retrograde tracer into the dorsolateral/lateral PAG resulted in (**J**) fluorescent retrograde labeling of neurons primarily in the CeM. **K:** Percentage and number of labeled neurons identified (n = 351 total) in the CeM and CeL following retrograde tracer injection into dorsolateral/lateral PAG. **L:** Retrograde tracer into the ventrolateral PAG resulted in (**M**) fluorescent retrograde labeling of neurons in both the CeM and CeL. **N:** Percentage and number of labeled neurons identified (n = 362 total) in the CeM and CeL following retrograde tracer injection into ventrolateral PAG. dm: dorsomedial, dl/l: dorsolateral/lateral, vl: ventrolateral, dr: dorsal nucleus raphe, BLA: basolateral amygdala.

This article is protected by copyright. All rights reserved.

Accepted Article

FIGURE 1

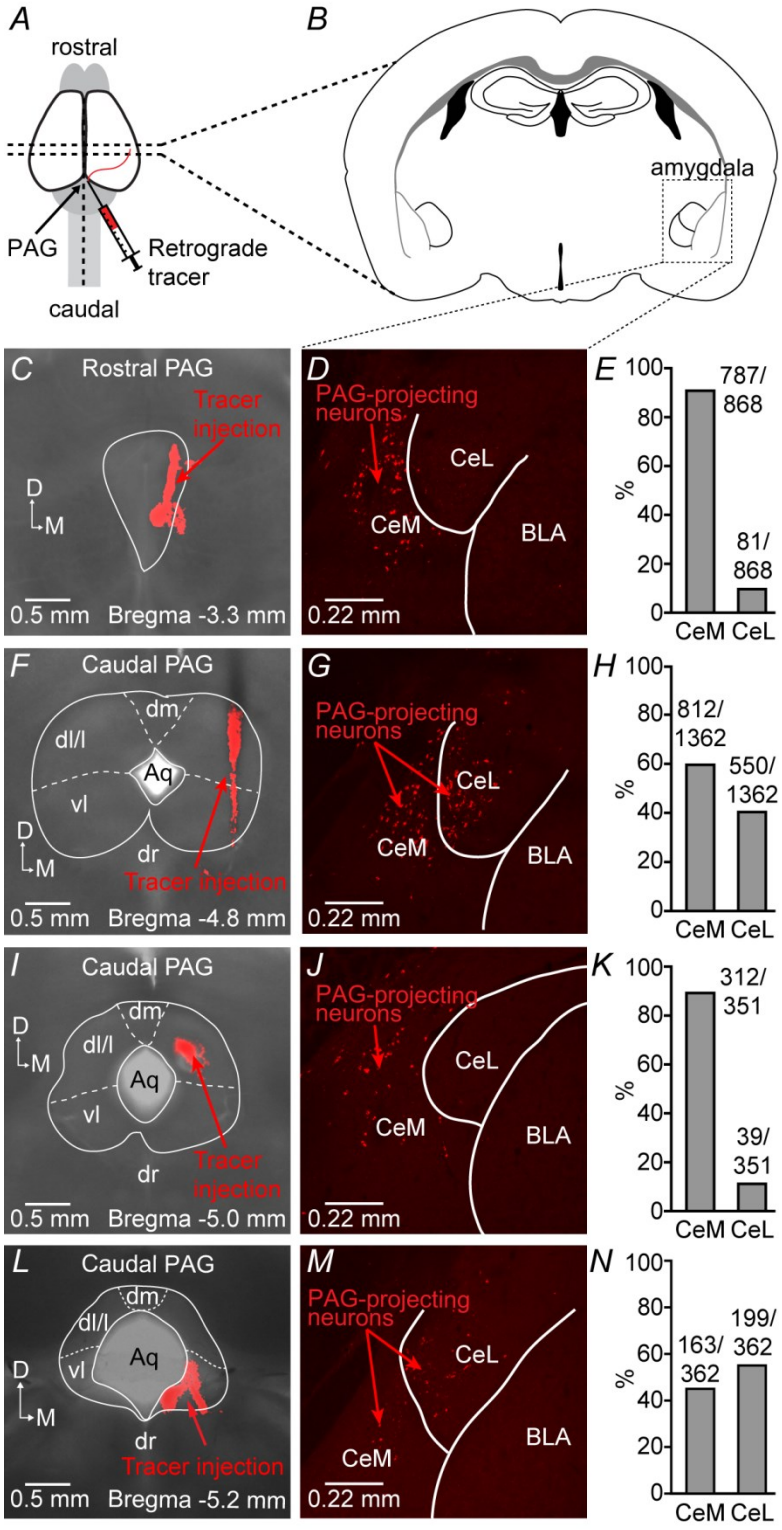

This article is protected by copyright. All rights reserved.

Accepted Article

Figure 2. A majority of PAG-projecting neurons in CeL are 'late-firing'.

A: Current-clamp recording from a 'late-firing' PAG-projecting CeL neuron showing the delayed onset of action potential (AP) generation at firing threshold (current steps: multiples of ± 50 pA). **B:** Current-clamp recording from a regular spiking PAG-projecting CeL neuron showing the rapid onset of AP generation at firing threshold (current steps: multiples of ± 50 pA). **C:** Plot of AP frequency vs. current injection values. **D:** Overlay of single AP traces (fAHP: fast afterhyperpolarization). **E-J:** Boxplots displaying comparisons of membrane potential, current threshold for AP firing, input resistance, AP frequency/current injection slope, fAHP, and onset time to first AP at firing threshold. *: $p < 0.05$; **: $p < 0.01$; ***: $p < 0.001$.

FIGURE 2

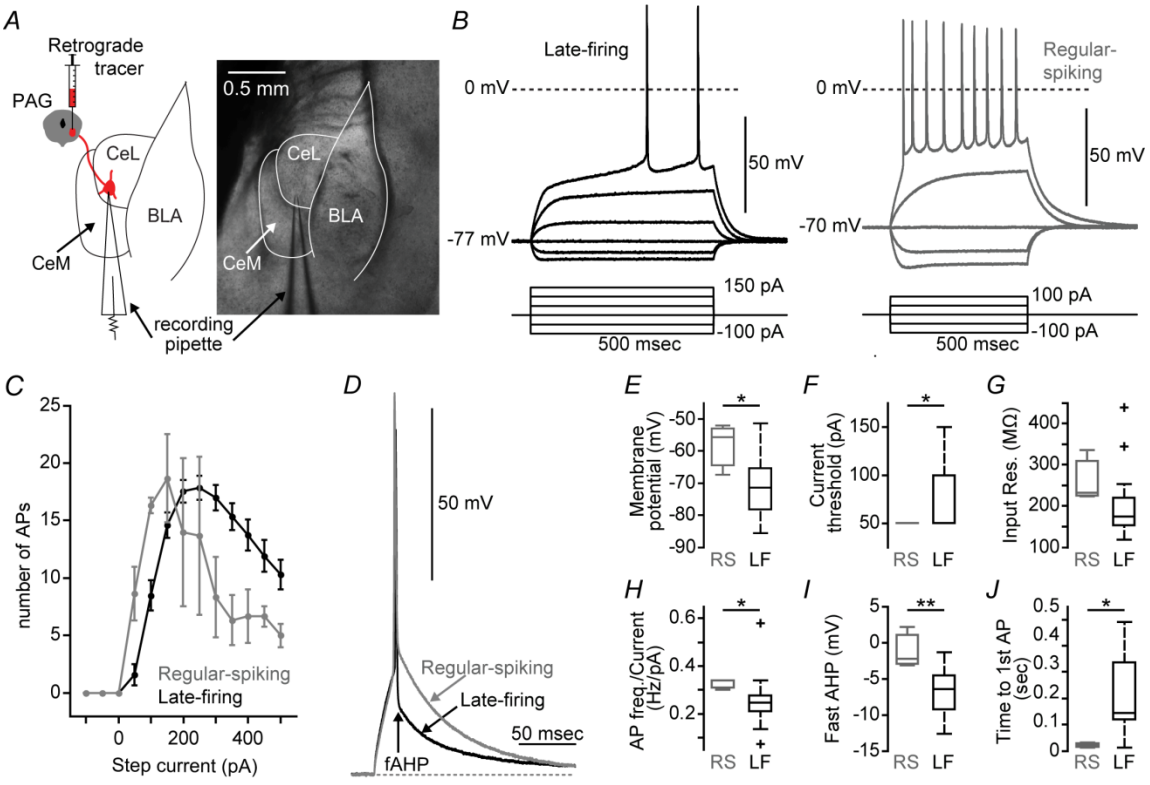

This article is protected by copyright. All rights reserved.

Accepted Article

Figure 3. PAG-projecting neurons in CeM are intrinsically heterogeneous.

A: Schematic depicting whole-cell recording of a retrogradely-labeled PAG-projecting neuron in the CeM. **B:** Example (4x bright-field video image) of a CeM-PAG recording in a brain slice. **C:** Proportion of distinct CeM-PAG subtypes identified by whole-cell electrophysiological recordings. **D-F:** Representative current-clamp traces of (i) a hyperpolarization current step to detect voltage sag, (ii) a single AP waveform, and (iii) trains of AP firing evoked by a 500 millisecond 100 pA step (bottom) and a 500 millisecond 300 pA step (top) for **(D)** fast-spiking, **(E)** bursting, and **(F)** regular-firing CeM-PAG neurons.

FIGURE 3

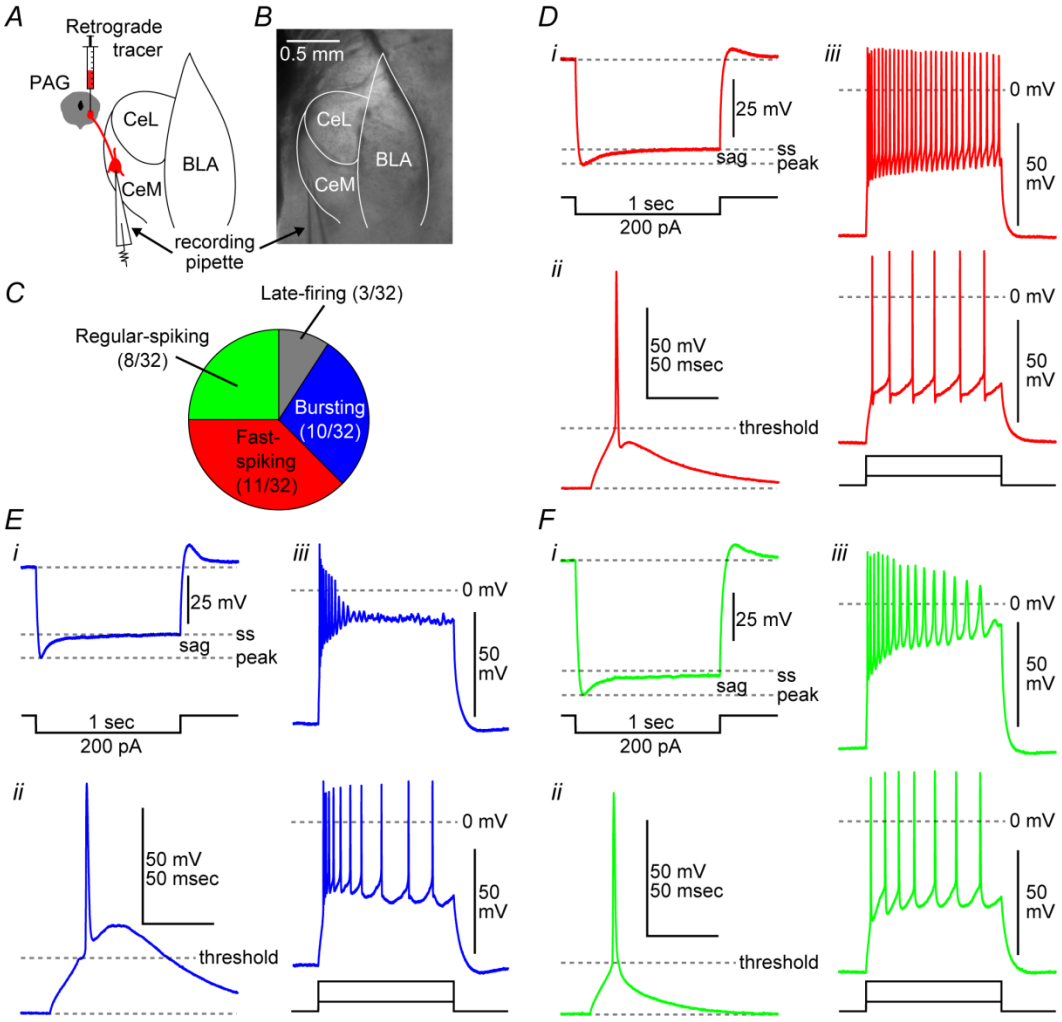

This article is protected by copyright. All rights reserved.

Accepted Article

Figure 4: Comparison of intrinsic properties for CeM-PAG subtypes.

A: Plot of AP frequency vs. current injection values for recorded CeM-PAG subtypes. **B-I:** Boxplots displaying comparisons of membrane potential, input resistance, voltage sag, current threshold for AP firing, voltage threshold for AP firing, spike-frequency adaptation, AP half-width, and fAHP (* = p ≤ 0.05, one-way ANOVA).

FIGURE 4

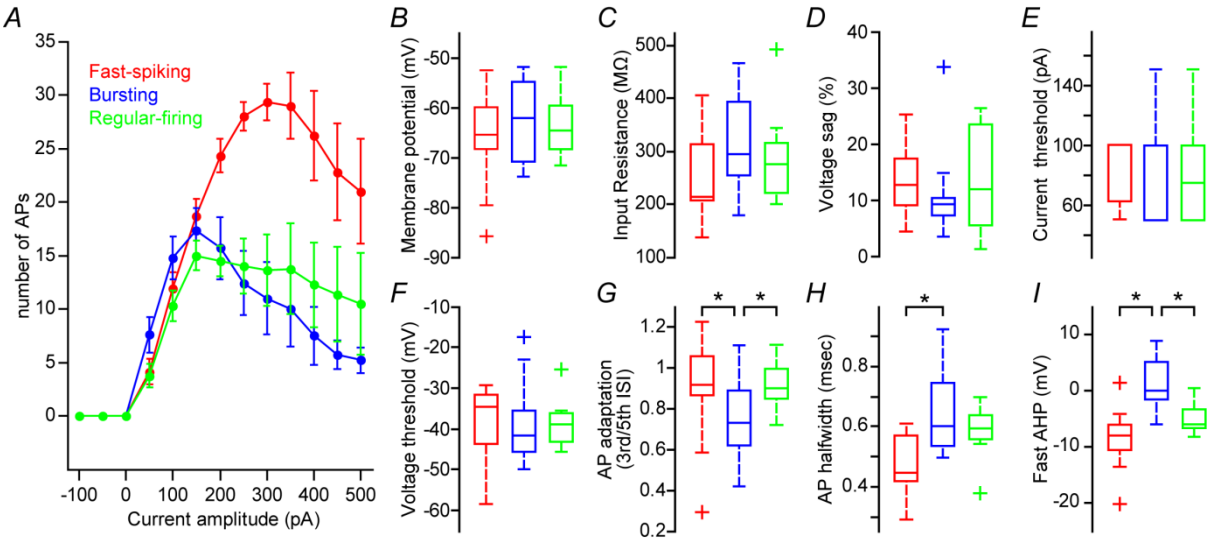

Figure 5: Excitability of late-firing CeL-PAG neurons is not altered 1 day after peripheral inflammatory insult.

A: Schematic of retrograde tracer injection into the PAG. **B:** Seven days following tracer injection into the PAG, saline or CFA was injected into the left hindpaw of littermates to induce peripheral inflammation. **C:** One day following CFA/saline injection (post-injection day 1: PID-1), CFA animals displayed significant allodynia compared to baseline (* p ≤ 0.05) and saline-injected littermates (# p ≤ 0.05, one-way ANOVA). **D:** Electrophysiological recordings were performed on CeL-PAG neurons on PID-1. **E:** Representing AP traces at firing threshold for late-firing CeL-PAG neurons recorded from a saline-injected (black) and CFA-

This article is protected by copyright. All rights reserved.

Accepted Article

injected (red) animal. **F:** Plot of AP frequency vs. current injection (left: resting membrane potential; right: holding membrane potential at -70 mV) for late-firing CeL-PAG neurons from saline-injected and CFA-injected mice. **G-K:** Boxplots displaying comparisons of membrane potential, input resistance, current threshold for AP firing, voltage threshold for AP firing, and onset of first AP at firing threshold (* = p ≤ 0.05).

FIGURE 5

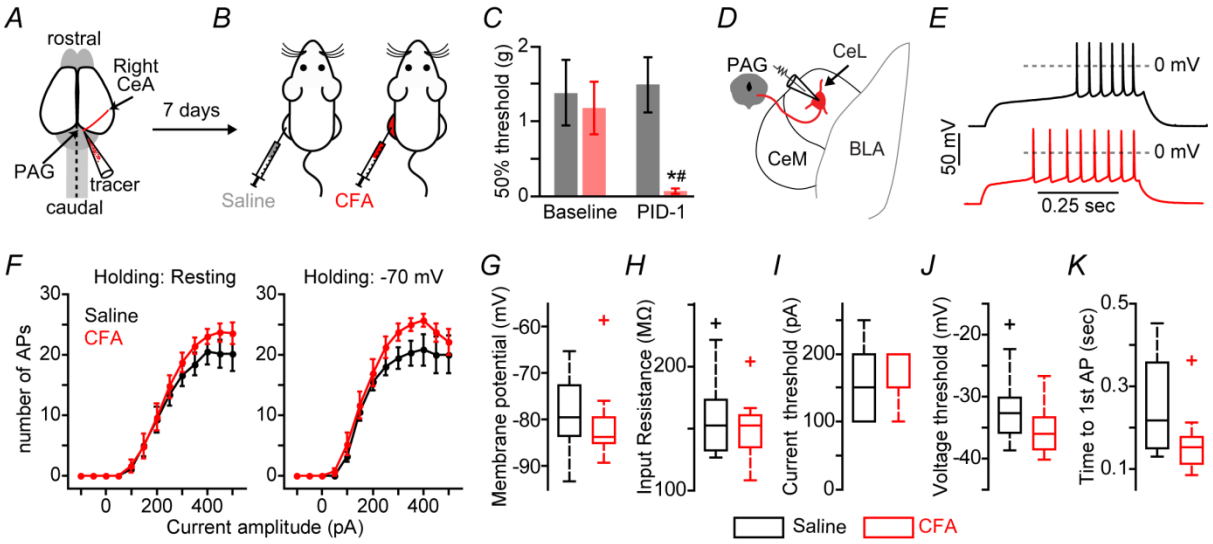

Figure 6: CeM-PAG subtypes are differentially altered 1 day after peripheral inflammatory insult.

A: One day following CFA/saline injection (post-injection day 1: PID-1), CFA animals displayed significant allodynia compared to baseline (* p ≤ 0.05) and saline-injected littermates (# p ≤ 0.05, one-way ANOVA). **B:** Electrophysiological recordings were performed on CeM-PAG neurons on PID-1. **C-E:** Representing AP traces at firing threshold for fast-spiking, regular-firing and bursting CeM-PAG neurons recorded from a saline-injected (black) and CFA-injected (red) animal. **F:** Plot of AP frequency vs. current injection (left: resting membrane potential; right: holding membrane potential at -70 mV) for fast-spiking CeM-PAG neurons from saline-injected and CFA-injected mice. **G-K:** Boxplots

This article is protected by copyright. All rights reserved.

Accepted Article

displaying comparisons of membrane potential, input resistance, voltage sag, current threshold for AP firing, voltage threshold for AP firing for fast-spiking CeM-PAG neurons. **L:** Plot of AP frequency vs. current injection (left: resting membrane potential; right: holding membrane potential at -70 mV) for regular-firing CeM-PAG neurons from saline-injected and CFA-injected mice. **M-Q:** Boxplots displaying comparisons of membrane potential, input resistance, voltage sag, current threshold for AP firing, voltage threshold for AP firing for regular-firing CeM-PAG neurons. **R:** Plot of AP frequency vs. current injection (left: resting membrane potential; right: holding membrane potential at -70 mV) for bursting CeM-PAG neurons from saline-injected and CFA-injected mice. **S-W:** Boxplots displaying comparisons of membrane potential, input resistance, voltage sag, current threshold for AP firing, voltage threshold for AP firing for bursting CeM-PAG neurons.*: $p < 0.05$; **: $p < 0.01$; ***: $p < 0.001$.

This article is protected by copyright. All rights reserved.

Accepted Article

FIGURE 6

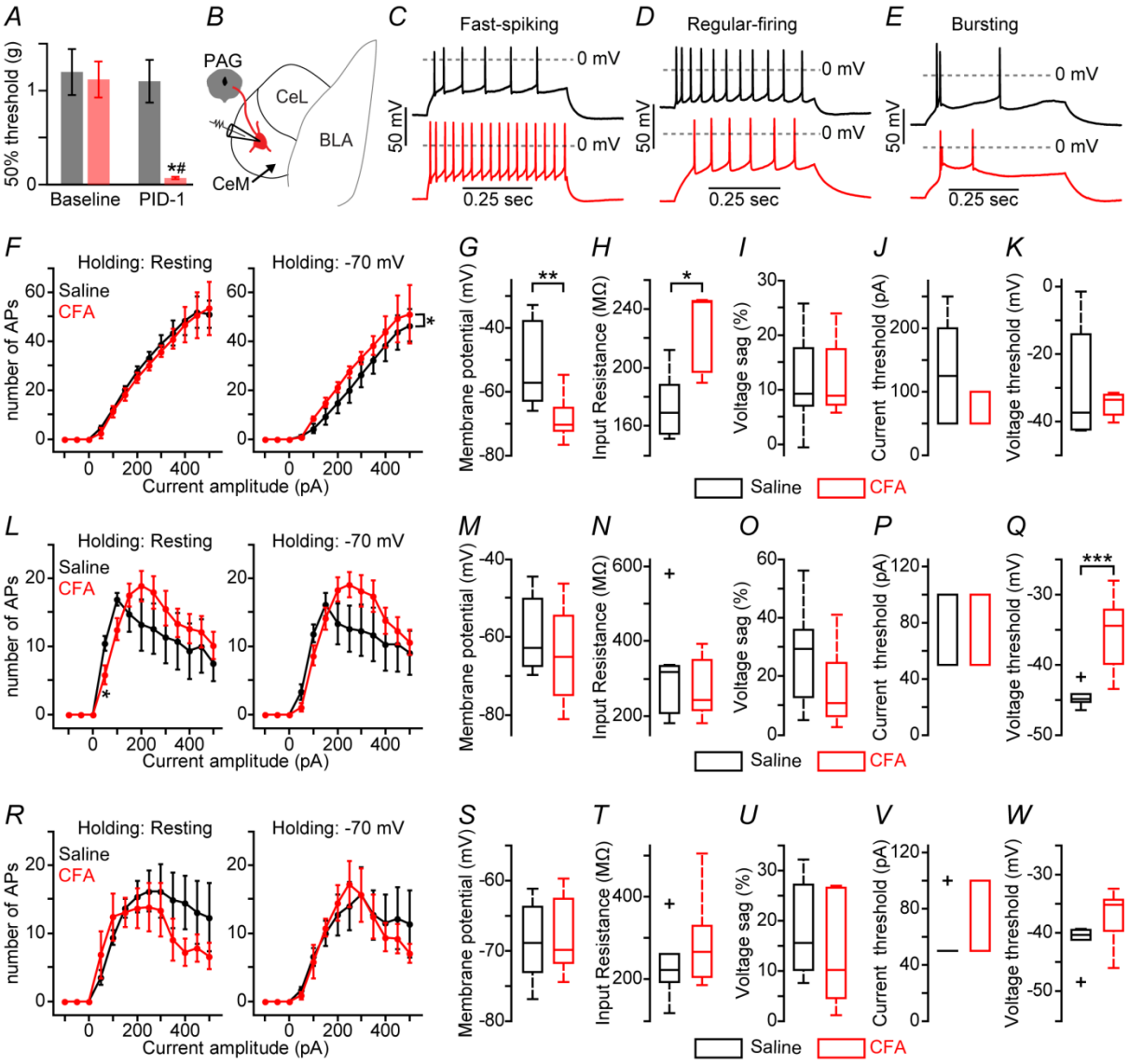

This article is protected by copyright. All rights reserved.

Accepted Article

Table 1: Intrinsic properties of neurons in the central amygdala that project to the periaqueductal gray

	CeM-PAG neurons	CeL-PAG neurons
	(n = 38, 24 animals, p25-p60)	(n = 30, 16 animals, p28-p40)
Tracer injection: PAG location	9 rostral, 15 caudal	16 caudal
	(8 entire caudal, 6 caudal dl/l, 1 caudal vl)	(12 entire caudal, 4 caudal vl)
Subthreshold properties		
Resting potential (mV)	-62.7 ± 1.3	-69.7 ± 1.8**#
Voltage sag (%)	12.6 ± 1.3	8.0 ± 1.3*$
Input resistance (MΩ)	262 ± 15	192 ± 11***$
Firing properties		
Voltage threshold (mV)	-39.0 ± 1.5	-34.0 ± 1.6*#
Current threshold (pA, 25Q-median-75Q)	50-100-100	50-100-100 ***$
Onset (msec)	47.5 ± 6.7	197 ± 28***$
Frequency/current (Hz/pA)	0.26 ± 0.02	0.26 ± 0.02
Half-width (msec)	0.57 ± 0.02	0.84 ± 0.05***$
Height (mV)	61.6 ± 1.8	73.0 ± 1.9***$
Spike frequency adaptation ($3^{rd}/5^{th}$)	0.83 ± 0.03	1.0 ± 0.03***$
Spike frequency adaptation ($5^{th}/10^{th}$)	0.82 ± 0.03	0.95 ± 0.02**$

*: $p < 0.05$; **: $p < 0.01$; ***: $p < 0.001$

#: Student's unpaired *t*-test

$: Wilcoxon rank sum test

25Q = First quartile (25^{th} percentile), 75Q = Third quartile (75^{th} percentile).

This article is protected by copyright. All rights reserved.

Accepted Article

Table 2: Intrinsic properties of CeL-PAG neuronal subtypes

	Late-firing neurons (n = 27, 14 of 16 mice, p28-p40)	Regular-spiking neurons (n = 3, 2 of 16 mice, p31-p38)
Tracer injection: PAG location	14 caudal (10 entire, 4 ventrolateral)	2 entire caudal
Subthreshold properties		
Resting potential (mV)	-71.2 ± 1.7	-58.4 ± 4.6*#
Voltage sag (%)	6.6 ± 1.2	15.3 ± 7.1*#
Input resistance (MΩ)	196 ± 17	264 ± 36
Firing properties		
Threshold (mV)	-34.5 ± 1.3	-42.8 ± 4.0
Onset (msec)	220 ± 27	22.8 ± 5.3**$
Frequency/current (Hz/pA)	0.25 ± 0.02	0.33 ± 0.01*$
Half-width (msec)	0.88 ± 0.05	0.54 ± 0.05*$
Height (mV)	72.2 ± 2.3	73.1 ± 2.1
Spike frequency adaptation ($3^{rd}/5^{th}$)	0.99 ± 0.03	1.07 ± 0.07
Spike frequency adaptation ($5^{th}/10^{th}$)	0.99 ± 0.02	0.99 ± 0.09
Fast afterhyperpolarization (mV)	5.2 ± 0.8	1.7 ± 2.1**#

* = p < 0.05; ** = p < 0.01; *** = p < 0.001

#: Student's unpaired *t*-test

$: Wilcoxon rank sum test

This article is protected by copyright. All rights reserved.

Accepted Article

Table 3: Intrinsic properties of CeM-PAG neuronal subtypes

	FS neurons (n = 11, 9 animals, p29-p41)	Bursting neurons (n = 10, 9 animals, p30-p41)	RS neurons (n = 8, 8 animals, p29-p60)	Significance
Tracer injection: PAG location	6 caudal (1 whole, 4 dl/l, 1 vl)	5 caudal (3 whole, 2 dl/l)	2 caudal (1 whole, 1 dl/l)	
	3 rostral	4 rostral	6 rostral	
Subthreshold properties				
Resting potential (mV)	-66.5 ± 3.5	-62.6 ± 2.8	-63.5 ± 2.3	none$^{\#}$
Voltage sag (%)	13.3 ± 1.8	18.3 ± 3.0	13.6 ± 3.5	none^
Input resistance (MΩ)	249 ± 24	306 ± 29	290 ± 33	none$^{\#}$
Firing properties				
Threshold (mV)	-38.1 ± 2.7	-38.1 ± 3.3	-38.5 ± 2.2	none$^{\#}$
Onset (msec)	48.2 ± 6.4	37.3 ± 4.2	40.2 ± 9.1	none$^{\#}$
Frequency/current (Hz/pA)	0.25 ± 0.02	0.31 ± 0.03	0.21 ± 0.03	none^
Half-width (msec)	0.46 ± 0.03	0.65 ± 0.05	0.58 ± 0.03	a, c$^{\#}$
Height (mV)	64.5 ± 3.0	63.8 ± 2.9	52.7 ± 3.2	c$^{\#}$
Spike frequency adaptation ($3^{rd}/5^{th}$)	0.89 ± 0.08	0.74 ± 0.06	0.91 ± 0.04	a, b^
Spike frequency adaptation ($5^{th}/10^{th}$)	0.89 ± 0.04	0.66 ± 0.08	0.81 ± 0.05	a$^{\#}$
Fast afterhyperpolarization	-8.5 ± 1.7	1.3 ± 1.4	-4.9 ± 1.0	a, b$^{\#}$

This article is protected by copyright. All rights reserved.

Accepted Article

(mV)

FS, fast-spiking; RS, regular-spiking. Data shown as mean ± standard error of the mean. a, FS vs Bursting; b, Bursting vs RS; c, FS vs RS. #ANOVA (normally distributed data) or ^Kruskal-Wallace test (non-normally distributed data) followed by a Bonferroni post-hoc analysis for multiple comparisons was used to determine statistical significance which was set at $p < 0.05$.

Table 4: Comparison of intrinsically distinct CeA-PAG neurons based on sex

	CeM FS neurons		CeM Bursting neurons		CeM RS neurons		CeL LF neurons	
	Male (n = 9)	Female (n = 4)	Male (n = 5)	Female (n = 5)	Male (n = 5)	Female (n = 3)	Male (n = 10)	Female (n = 17)
Subthreshold properties								
Resting potential (mV)	-64.0 ± 3.6	-65.7 ± 6.8	-58.1 ± 3.0	-63.6 ± 3.0	-63.1 ± 1.1	-60.1 ± 3.8	-67.9 ± 1.5	***-74.4 ± 1.6**#***
Voltage sag (%)	15.3 ± 2.5	10.0 ± 1.5	8.51 ± 1.8	13.9 ± 5.0	16.4 ± 4.1	8.8 ± 6.4	2.7 ± 1.7	***9.2 ± 1.3**#***
Input resistance (MΩ)	248 ± 34	251 ± 34	307 ± 24	306 ± 55	270 ± 23	324 ± 87	180 ± 17	186 ± 13
Firing properties								
Threshold (mV)	-37.6 ± 2.5	-39.2 ± 6.5	-36.6 ± 3.9	-39.6 ± 5.8	-39.5 ± 1.8	-36.9 ± 5.7	-27.3 ± 2.7	***-37.3 ± 1.0***$***
Onset (msec)	50.8 ± 9.2	43.5 ± 8.5	32.8 ± 0.7	41.8 ± 0.4	46.2 ± 13	30.0 ± 9.1	232 ± 41	195 ± 32
Frequency/current (Hz/pA)	0.23 ± 0.03	0.28 ± 0.04	0.32 ± 0.05	0.30 ± 0.05	0.18 ± 0.01	0.26 ± 0.07	0.21 ± 0.02	0.26 ± 0.02
Half-width (msec)	0.51 ± 0.03	***0.38 ± 0.05*#***	0.65 ± 0.07	0.63 ± 0.07	0.63 ± 0.02	0.50 ± 0.07	0.98 ± 0.1	***0.79 ± 0.04**$***

This article is protected by copyright. All rights reserved.

Accepted Article

Height (mV)	66.8 ± 4.6	60.5 ± 1.5	66.2 ± 4.1	61.4 ± 4.3	55.2 ± 4.8	48.4 ± 2.6	62.3 ± 4.7	***76.5 ± 2.0**#***
SFA ($3^{rd}/5^{th}$)	0.87 ± 0.11	0.92 ± 0.13	0.76 ± 0.06	0.60 ± 0.05	0.94 ± 0.07	0.87 ± 0.03	1.04 ± 0.05	1.03 ± 0.04
SFA ($5^{th}/10^{th}$)	0.89 ± 0.06	0.87 ± 0.05	0.75 ± 0.09	0.58 ± 0.12	0.79 ± 0.07	0.86 ± 0.07	0.96 ± 0.04	0.95 ± 0.03
fAHP (mV)	-8.3 ± 2.5	-8.9 ± 1.6	0.2 ± 2.1	2.4 ± 2.0	-5.8 ± 1.1	-3.5 ± 2.1	-7.9 ± 1.2	***-4.3 ± 1.0*$***

FS, fast-spiking; RS, regular-spiking; LF, late-firing. Data shown as mean ± standard error of the mean.

* = p < 0.05; ** = p < 0.01; *** = p < 0.001

#: Student's unpaired *t*-test

$: Wilcoxon rank sum test

Table 5: CeA-subtypes based on injection location of retrograde tracer within the PAG of naïve mice

	CeM-PAG neurons				CeL-PAG neurons	
Injection location	**Fast-spiking**	**Bursting**	**Regular-spiking**	**Late-firing**	**Regular-spiking**	**Late-firing**
Rostral PAG	3/11 (27%)	5/10 (50%)	6/8 (75%)	0/3 (0%)	0/3 (0%)	0/27 (0%)
Caudal PAG (whole)	1/11 (9%)	1/10 (10%)	0/8 (%)	3/3 (100%)	3/3 (100%)	14/27 (52%)
Caudal PAG (dl/l)	6/11 (55%)	4/10 (40%)	2/8 (25%)	0/3 (0%)	0/3 (0%)	0/27 (0%)
Caudal PAG (vl)	1/11 (9%)	0/10 (0%)	0/8 (%)	0/3 (0%)	0/3 (0%)	13/27 (48%)

This article is protected by copyright. All rights reserved.

Accepted Article

Table 6: Intrinsic properties of CeL-PAG late firing neurons in CFA inflammatory pain model

	Saline-injection (n = 10 neurons, 5 animals, p35-p51)	CFA-injection (n = 11 neurons, 7 animals, p30-p50)
Tracer injection: PAG location	5 caudal (1 entire caudal PAG, 4 caudal vlPAG)	7 caudal (2 entire caudal PAG, 5 caudal vlPAG)
Subthreshold properties		
Resting potential (mV)	-78.9 ± 2.7	-81.0 ± 2.5
Voltage sag (%)	3.9 ± 1.0	4.9 ± 1.1
Input resistance (MΩ)	161 ± 13	149 ± 7.8
Firing properties		
Threshold (mV)	-31.5 ± 2.1	-35.4 ± 1.2
Onset (msec)	264 ± 39	165 ± 28*
Frequency/current (Hz/pA)	0.18 ± 0.02	0.21 ± 0.02
Half-width (msec)	0.82 ± 0.08	0.72 ± 0.04
Height (mV)	69.6 ± 3.4	74.3 ± 2.1
Spike frequency adaptation ($3^{rd}/5^{th}$)	1.02 ± 0.03	1.11 ± 0.03
Spike frequency adaptation ($5^{th}/10^{th}$)	1.0 ± 0.02	1.1 ± 0.01
Fast afterhyperpolarization (mV)	8.4 ± 0.5	7.8 ± 0.6

Data shown as mean ± standard error of the mean. *: p = 0.057

This article is protected by copyright. All rights reserved.

Accepted Article

Table 7: Intrinsic properties of CeM-PAG neuronal subtypes in CFA inflammatory pain model

	FS neurons		Bursting neurons		RS neurons	
	Saline (n = 5 neurons, 3 animals, p27-p51)	CFA (n = 5 neurons, 4 animals, p30-p41)	Saline (n = 6 neurons, 3 animals, p30-p51)	CFA (n = 5 neurons, 4 animals, p27-p51)	Saline (n = 7 neurons, 5 animals, p29-p41)	CFA (n = 14 neurons, 9 animals, p28-p51)
Tracer injection: PAG location	3 caudal (1 entire caudal, 1 caudal dl/l, 1 caudal vl)	2 caudal, 2 rostral (1 caudal dl/l, 1 caudal vl)	1 caudal dl/l, 2 rostral	2 caudal, 2 rostral (1 entire caudal, 1 caudal dl/l)	3 caudal, 2 rostral (2 entire caudal, 1 caudal dl/l)	6 caudal, 3 rostral (2 entire caudal, 2 caudal dl/l, 2 caudal vl)
Subthreshold properties						
Resting potential (mV)	-50.3 ± 6.3	-68.3 ± 3.6**#	-67.3 ± 2.6	-63.4 ± 2.8	-59.1 ± 3.0	-63.7 ± 2.8
Voltage sag (%)	10.1 ± 4.3	12.2 ± 3.3	17.9 ± 4.1	14.1 ± 5.3	27.1 ± 6.5	15.3 ± 3.1
Input resistance (MΩ)	175 ± 11	224 ± 12*$	233 ± 36	288 ± 56	310 ± 51	269 ± 19
Firing properties						
Threshold (mV)	-26.3 ± 8.0	-35.4 ± 2.3	-41.5 ± 1.4	-37.2 ± 2.3	-44.6 ± 0.6	-35.8 ± 1.4***#
Onset (msec)	67.2 ± 13.5	45.2 ± 11.3	0.04 ± 0.004	45.2 ± 11.3	23.4 ± 4.6	48.6 ± 5.8**#
Frequency/current (Hz/pA)	0.3 ± 0.02	0.3 ± 0.04	0.2 ± 0.02	0.2 ± 0.07	0.3 ± 0.02	0.3 ± 0.02

This article is protected by copyright. All rights reserved.

Accepted Article

Half-width (msec)	0.3 ± 0.04	0.4 ± 0.05	0.7 ± 0.1	0.5 ± 0.04	0.5 ± 0.02	0.5 ± 0.02
Height (mV)	58.2 ± 2.0	66.5 ± 6.4	69.2 ± 6.4	70.3 ± 4.3	70.2 ± 3.0	63.5 ± 3.4
Spike frequency adaptation ($3^{rd}/5^{th}$)	1.0 ± 0.1	0.8 ± 0.2	0.9 ± 0.1	0.7 ± 0.09	0.9 ± 0.06	0.9 ± 0.06
Spike frequency adaptation ($5^{th}/10^{th}$)	0.8 ± 0.2	0.9 ± 0.04	0.8 ± 0.05	0.7 ± 0.1	0.8 ± 0.04	0.9 ± 0.07
Fast afterhyperpolarization (mV)	8.8 ± 2.4	12.0 ± 1.0	2.7 ± 1.4	0.6 ± 1.5	3.2 ± 1.5	8.8 ± 2.1

FS, fast-spiking; RS, regular-spiking. Data shown as mean ± standard error of the mean.

Statistical comparisons are for saline vs. CFA; *: $p < 0.05$; **: $p < 0.01$; ***: $p < 0.001$

#: Student's unpaired *t*-test

$: Wilcoxon rank sum test

Table 8: CeA-subtypes based on injection location of retrograde tracer within the PAG of saline and CFA-injected mice

	CeM-PAG neurons								CeL-PAG neurons			
Injection location	**Fast-spiking**		**Bursting**		**Regular-spiking**		**Late-firing**		**Regular-spiking**		**Late-firing**	
	Saline	CFA	Saline	CFA	Saline	CFA	Saline	CFA	Saline	CFA	Saline	CFA
	5/19 (26.3 %)	5/25 (20 %)	6/19 (31.6 %)	5/25 (20 %)	7/19 (36.8 %)	14/25 (56%)	1/19 (5.3 %)	1/25 (4%)	1/11 (9.1 %)	2/13 (15.4 %)	10/11 (90.9 %)	11/13 (84.6 %)
Rostral PAG	0/5 (0%)	3/5 (80 %)	5/6 (83.3 %)	4/5 (80 %)	5/7 (71.4 %)	3/14 (21.4 %)	0/1 (0%)	0/1 (0%)	0/1 (0%)	0/2 (0%)	0/10 (0%)	0/11 (0%)

This article is protected by copyright. All rights reserved.

Accepted Article

Caudal PAG (whole)	0/5 (0%)	0/5 (0%)	0/6 (0%)	0/5 (0%)	1/7 (14.3%)	6/14 (42.8%)	1/1 (100%)	1/1 (100%)	1/1 (100%)	0/2 (0%)	2/10 (20%)	2/11 (18.2%)
Caudal PAG (dl/l)	4/5 (80%)	1/5 (20%)	1/6 (16.7%)	1/5 (20%)	1/7 (14.3%)	3/14 (21.4%)	0/1 (0%)	0/1 (0%)	0/1 (0%)	0/2 (0%)	0/10 (0%)	0/11 (0%)
Caudal PAG (vl)	1/5 (20%)	1/5 (20%)	0/6 (0%)	0/5 (0%)	0/7 (0%)	2/14 (14.2%)	0/1 (0%)	0/1 (0%)	0/1 (0%)	2/2 (100%)	8/10 (80%)	9/11 (81.8%)

Jun-Nan Li is a post-doctoral fellow working in the Sheets lab at Stark Neurosciences Research Institute and Department of Pharmacology and Toxicology of Indiana University School of Medicine. He obtained his PhD in Pharmacology from the Harbin Medical University in China. He trained in electrophysiology with Showalter professor of Pharmacology Grant D. Nicol at Indiana University. His current research interests are using cutting edge technology to dissect the neural circuits involved in pain. His goal is to run his own lab aimed at dissecting and manipulating neural circuits modulating the autonomic function and emotion.

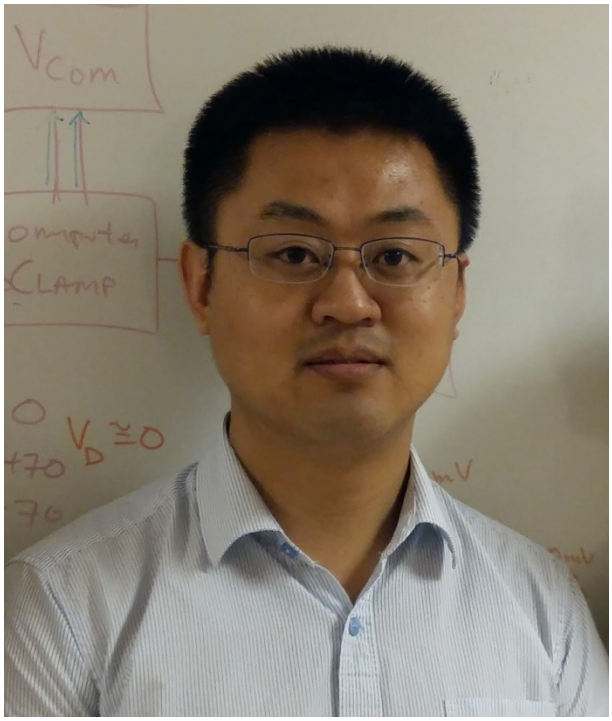

This article is protected by copyright. All rights reserved.